Supporting Information

Aqueous CO_2 Electroreduction with Amine-Decorated Manganese Bipyridine Complexes Immobilized on Carbon Nanotubes

Lin Li,[a,‡] Wanwan Hong,[b,‡] Afsaneh Azhdeh,[c] Joakim B. Jakobsen,[a,†] Steen U. Pedersen,[a] and Kim Daasbjerg[a,*]

[a] Novo Nordisk Foundation (NNF) CO_2 Research Center, Department of Chemistry, Aarhus University, Gustav Wieds Vej 10C, 8000 Aarhus C, Denmark

[b] Zhongyuan Critical Metals Laboratory, Zhengzhou University, Zhengzhou 450001, China

[c] Faculty of Chemistry, Kharazmi University, Tehran, Iran

[†] Present address: Department of Drug Design and Pharmacology, University of Copenhagen, Jagtvej 162, 2100 Copenhagen Ø, Denmark

[‡] L.L. and W.H. contributed equally to the work.

*Correspondence to: kdaa@chem.au.dk

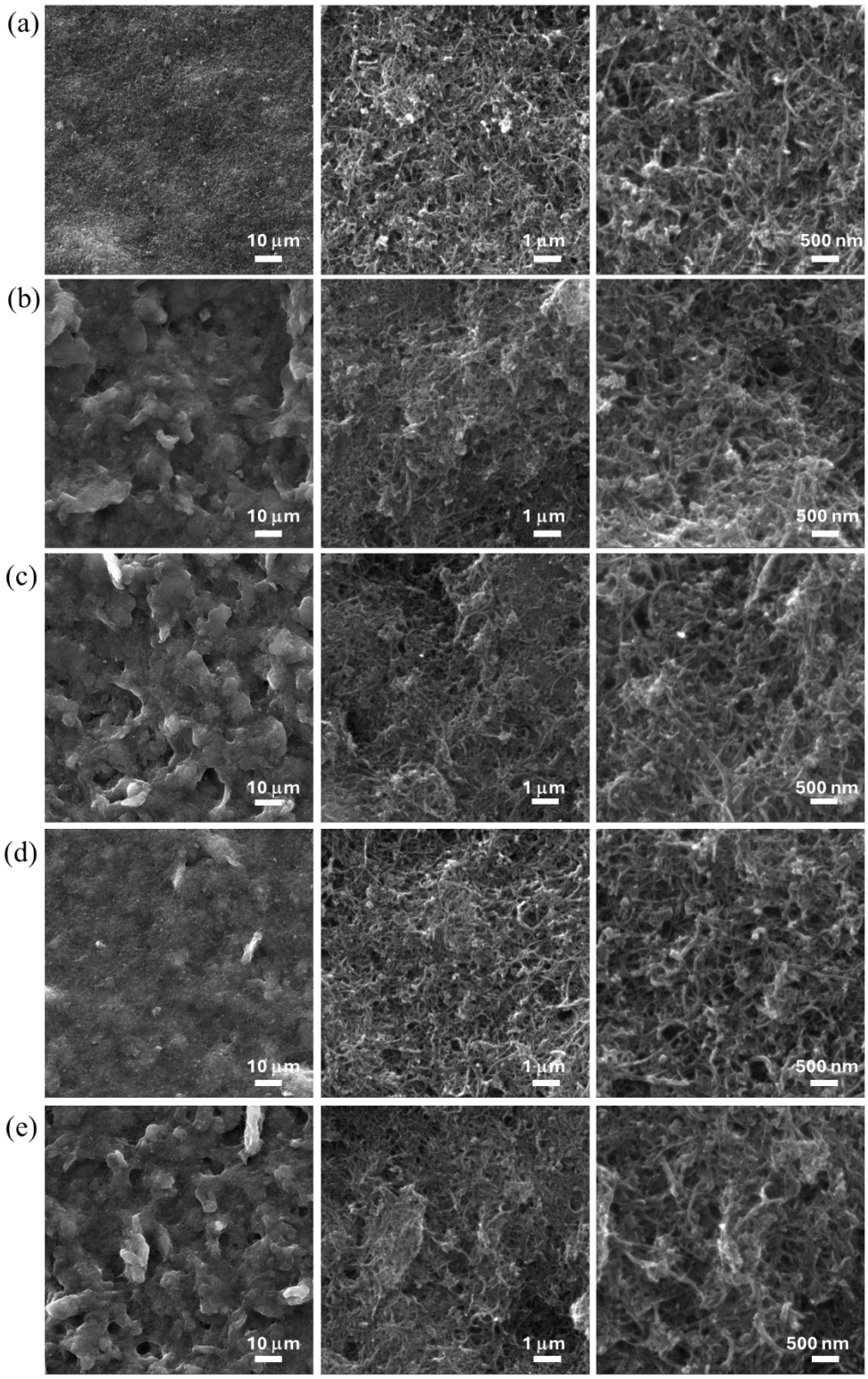

Figure S1. SEM images of (a) blank MWCNT, (b) **I**/MWCNT, (c) **II**/MWCNT, (d) **III**/MWCNT, and (e) **IV**/MWCNT electrodes.

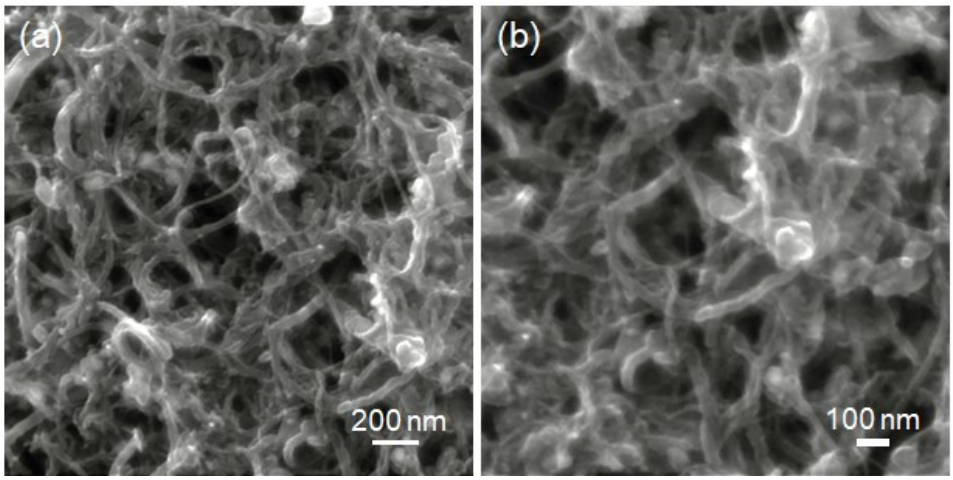

Figure S2. High-magnification SEM images of **III**/MWCNT.

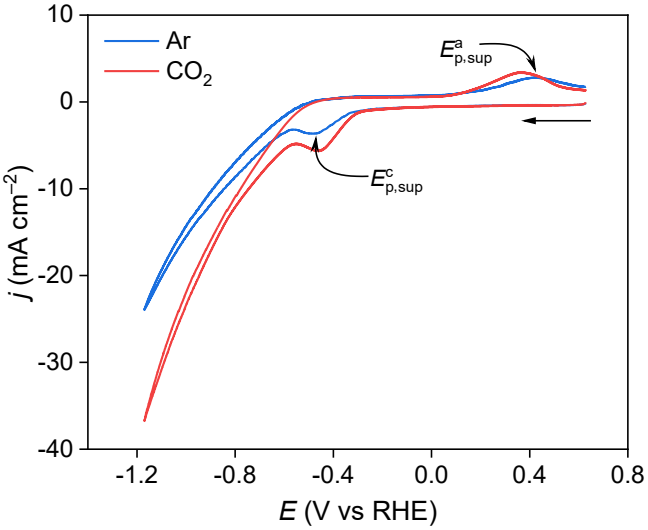

Figure S3. Cyclic voltammograms recorded on **I**/MWCNT using a sweep rate of 0.1 V s^{-1} in Ar-saturated (blue trace) and CO_2-saturated (red trace) 0.5 M $KHCO_3$.

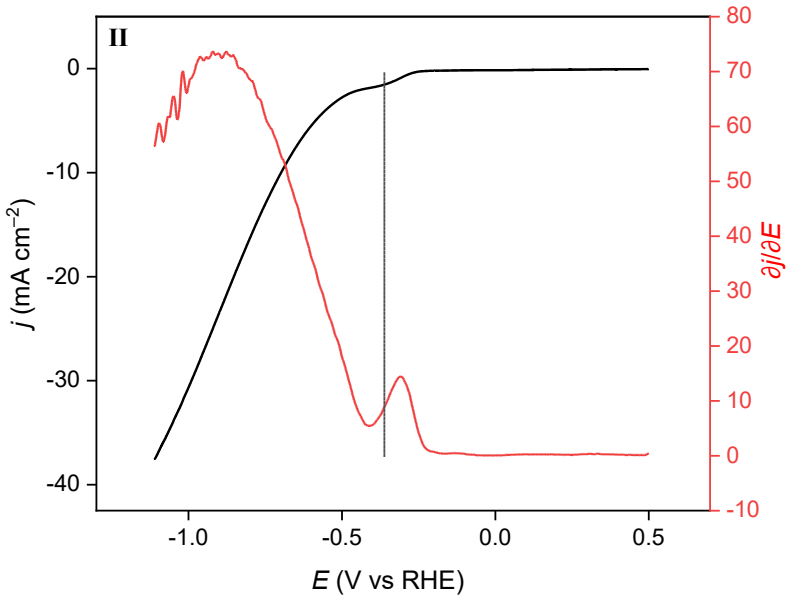

Figure S4. Linear sweep voltammogram recorded on **II**/MWCNT using a sweep rate of 0.1 V s^{-1} in Ar-saturated 0.5 M $KHCO_3$ (black curve) and the first derivative of the current density with respect to potential ($\partial j/\partial E$) (red curve). The midpoint of the local maximum and minimum positions of the derivative plot features the reduction potential of the bump in the voltammogram at –0.36 V vs RHE (dotted line).

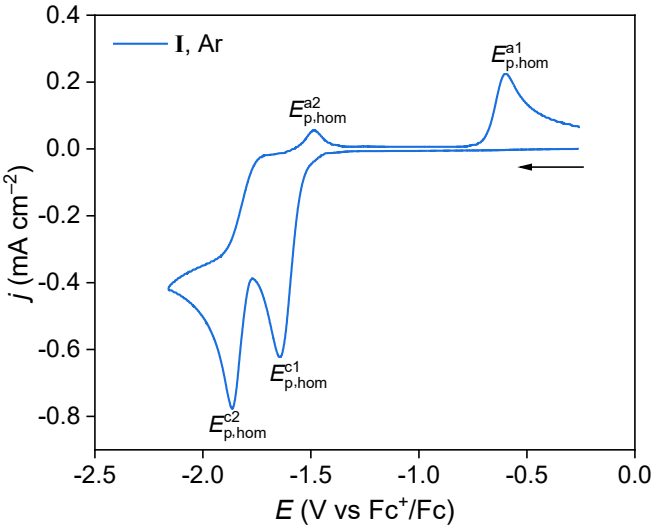

Figure S5. Cyclic voltammograms recorded on 1 mM of complex **I** at a glassy carbon electrode (diameter = 1 mm) using a sweep rate of 0.1 V s^{-1} in Ar-saturated 0.1 M Bu_4NBF_4/acetonitrile.

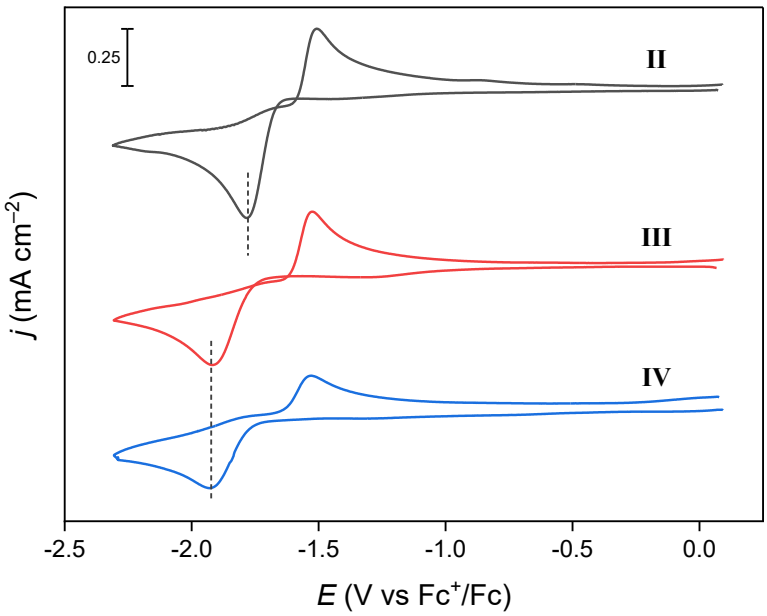

Figure S6. Cyclic voltammograms recorded on 1 mM of complexes **II–IV** at a glassy carbon electrode (diameter = 1 mm) using a sweep rate of 0.1 V s^{-1} in Ar-saturated 0.1 M Bu_4NBF_4/acetonitrile.

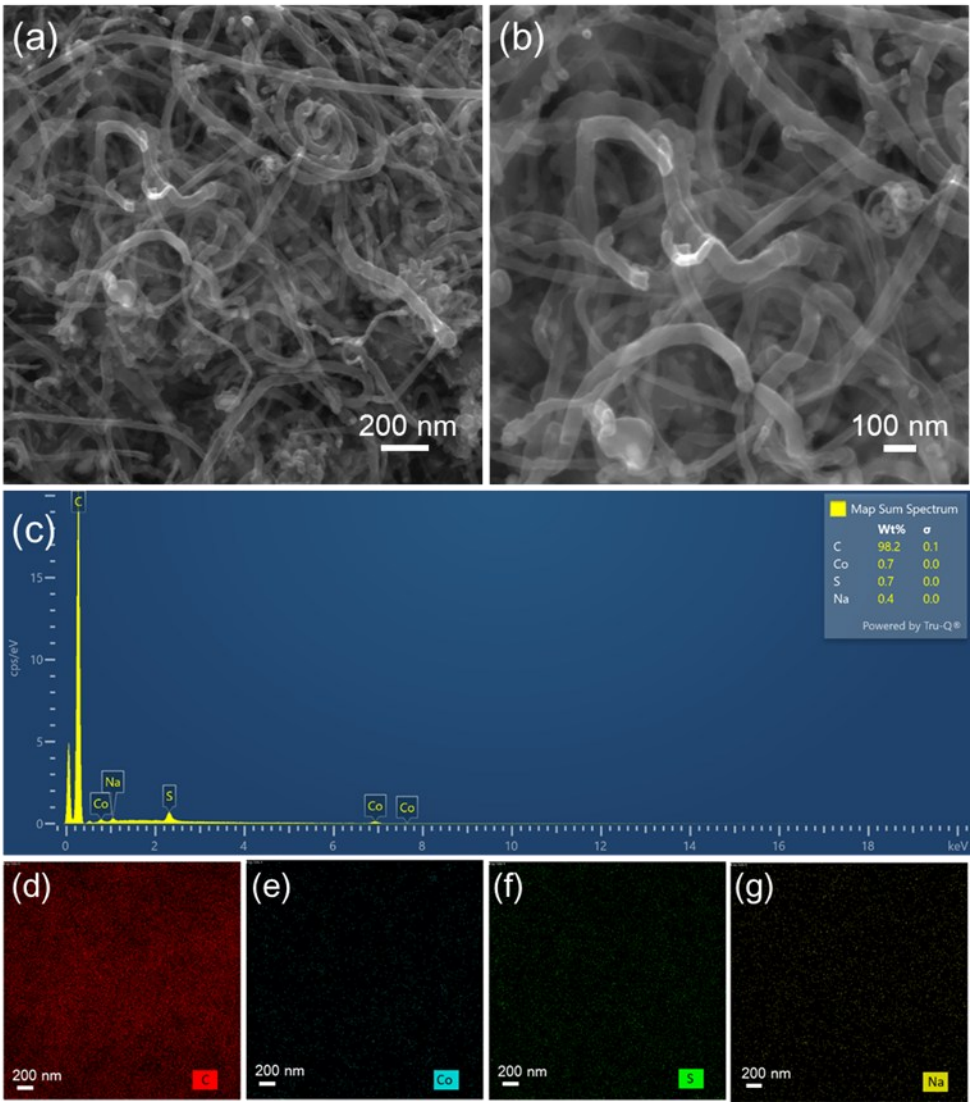

Figure S7. SEM images (a, b), EDX sum spectrum (c), and corresponding EDX elemental mappings (d–f) for C (red), Co (cyan), S (green), and Na (yellow) for pristine MWCNT.

SEM/EDX analysis of pristine MWCNT reveals trace Co (0.7 wt%), attributable to residual Co catalyst from CVD synthesis, along with minor S and Na from post-treatment processes. CPE on a blank MWCNT electrode shows negligible current, with all charge consumed producing only H_2 (**Table S1**). These results confirm that residual metals contribute no significant catalytic activity.

Table S1. Product Distribution Obtained for Blank MWCNT and **I–IV**/MWCNT after 15 min CPE in CO_2-Saturated 0.5 M $KHCO_3$.

Catalyst	*E* (V vs RHE)	**I–IV**/MWCNT mass ratio	Charge (C)	FE (%) CO	FE (%) HCOOH	FE (%) H_2
MWCNT	–0.67	-	0.48 ± 0.01	-	-	100
I/MWCNT	–0.67	0.3	0.54 ± 0.02	43 ± 4	20 ± 5	31 ± 3
I/MWCNT	–0.67	0.8	0.54 ± 0.03	26 ± 1	13 ± 0	52 ± 2
I/MWCNT	–0.67	1.3	0.81 ± 0.13	35 ± 6	31 ± 8	38 ± 5
II/MWCNT	–0.67	0.8	6.41 ± 0.32	4 ± 0	63 ± 4	26 ± 1
III/MWCNT	–0.47	0.8	1.37 ± 0.02	2 ± 0	48 ± 1	16 ± 0
III/MWCNT	–0.57	0.8	3.51 ± 0.13	4 ± 0	57 ± 2	21 ± 1
III/MWCNT	–0.67	0.8	7.92 ± 0.06	3 ± 0	72 ± 1	23 ± 0
III/MWCNT	–0.77	0.8	7.85 ± 0.09	4 ± 0	63 ± 1	28 ± 1
III/MWCNT	–0.67	0.3	5.69 ± 0.01	4 ± 1	47 ± 5	39 ± 1
III/MWCNT	–0.67	0.6	3.79 ± 0.11	5 ± 0	64 ± 3	30 ± 3
III/MWCNT	–0.67	1.1	5.61 ± 0.61	5 ± 0	59 ± 4	28 ± 1
III/MWCNT	–0.67	1.3	5.17 ± 0.10	4 ± 0	65 ± 0	29 ± 0
IV/MWCNT	–0.57	0.8	0.56 ± 0.07	4 ± 0	17 ± 4	75 ± 1
IV/MWCNT	–0.67	0.8	3.18 ± 0.05	1 ± 0	13 ± 1	81 ± 2
IV/MWCNT	–0.77	0.8	3.23 ± 0.53	2 ± 0	13 ± 1	87 ± 1

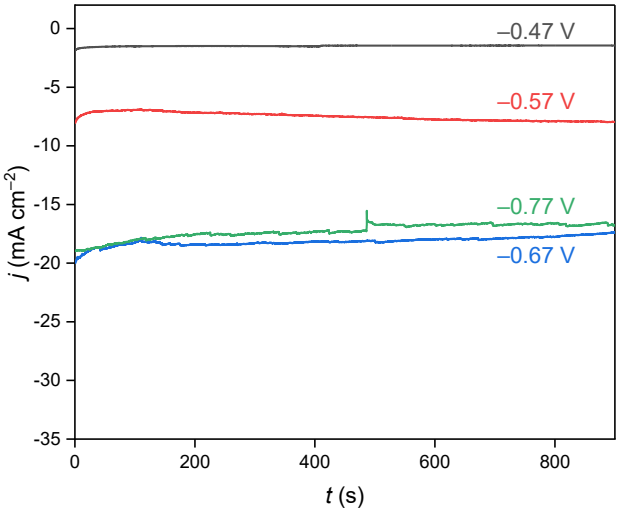

Figure S8. Current density recorded for **III**/MWCNT at various potentials during 15 min electrolysis in CO_2-saturated 0.5 M $KHCO_3$.

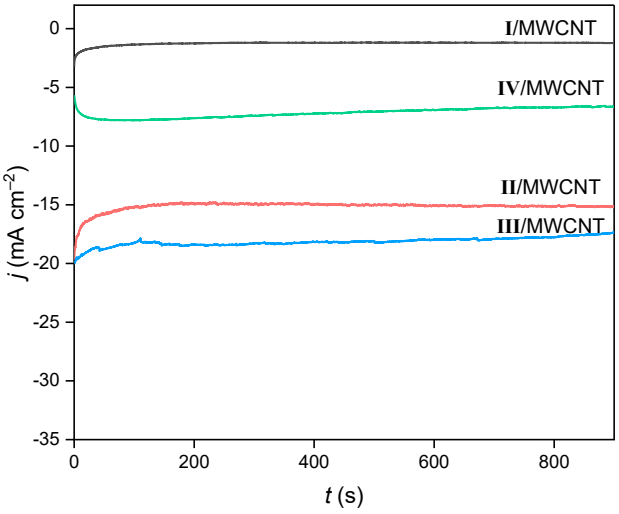

Figure S9. Current density recorded for **I–IV**/MWCNT at –0.67 V vs RHE during 15 min electrolysis in CO_2-saturated 0.5 M $KHCO_3$.

Table S2. Product Distribution Obtained for Complexes **I–IV** after 1 h Controlled Potential Electrolysis in CO_2-saturated 0.2 M Bu_4NBF_4/acetonitrile.

Complex	*E* (V vs Fc^+/Fc)	Additive	FE (%) CO	FE (%) HCOOH	FE (%) H_2	Ref
I	–1.70	5% H_2O	100	-	-	S1
II	–2.17	2.0 M TFE	12.5	63	5.5	S2
III	–2.17	2.0 M TFE	4.8	71	6.4	S2
IV	–2.15	1.0 M PhOH	1	16	64	S3
IV	–2.15	2.0 M TFE	2	44	53	S3
IV	–2.15	1.0 M *i*PrOH	1	81	3	S3

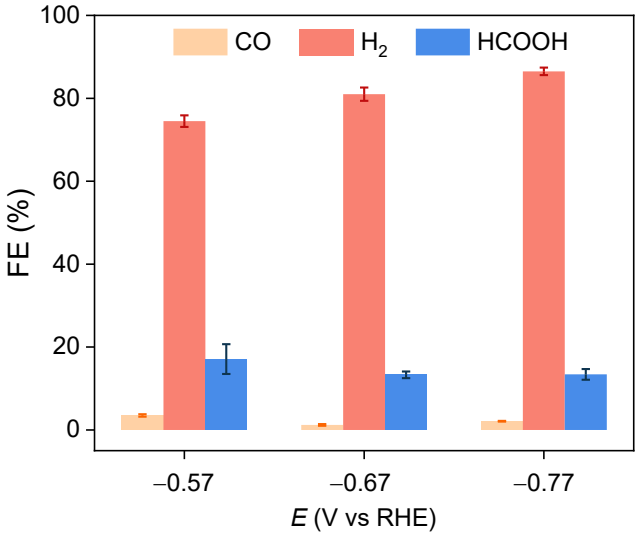

Figure S10. FEs of various products on **IV**/MWCNT at different applied potentials after 15 min electrolysis in CO_2-saturated 0.5 M $KHCO_3$ (mass ratio of **IV** to MWCNT = 0.8). Error bars correspond to the standard deviation of 2–3 independent measurements.

Table S3. Mn Concentration in Post-Electrolyte Determined by ICP.

	Mn concentration (μg/mL)	Total Mn concentration (μg/mL)[c]	Leaching ratio
Entry 1[a]	1.28	2.51	51.0%
Entry 2[b]	1.10	2.51	43.8%

[a]ICP analysis on the post-electrolyte for an electrolysis conducted using a **III**/MWCNT electrode at −0.67 V vs RHE in CO_2-saturated 0.5 M $KHCO_3$ (**Figure 7**). [b]ICP analysis on the post-electrolyte for a **III**/MWCNT electrode after 8 h stirring using the same setup as in **Entry 1** but without applying a potential. [c]Total Mn concentration represents the amount of Mn in the electrolyte if all deposited **III** catalyst on the electrode surface leaches into the electrolyte.

Catalyst leaching is observed both with and without the application of potential (entries 1 and 2, **Table S3**). This aligns with the fact that the Mn complexes on the MWCNT are oversaturated, with less than 25% of the total loaded Mn complex being electroactive (see discussion related to **Table S4**). During stirring, a portion of the electro-inactive complex detaches from the MWCNT and enters the electrolyte due to weak interactions. When a potential is applied, the Mn leaching ratio increases from 43.8% to 51.0%, indicating that the Mn complexes undergo somewhat greater detachment or deactivation under these conditions.

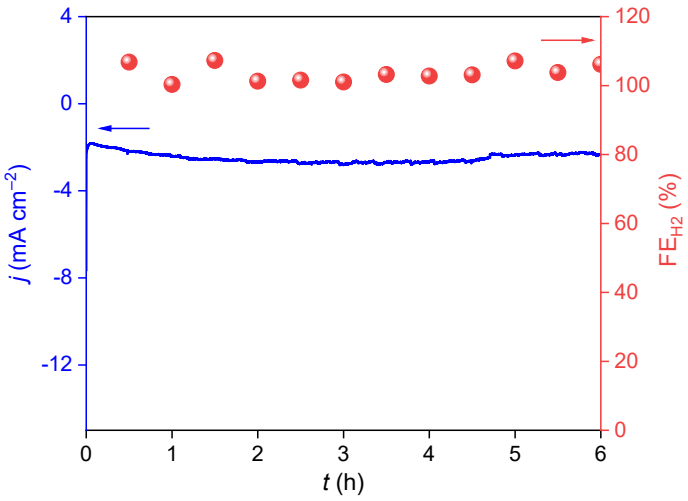

Figure S11. FE_{H2} and *j-t* curve recorded on blank MWCNT in the electrolyte recovered from the experiment in **Figure 7** at –0.67 V vs RHE in CO_2-saturated 0.5 M $KHCO_3$.

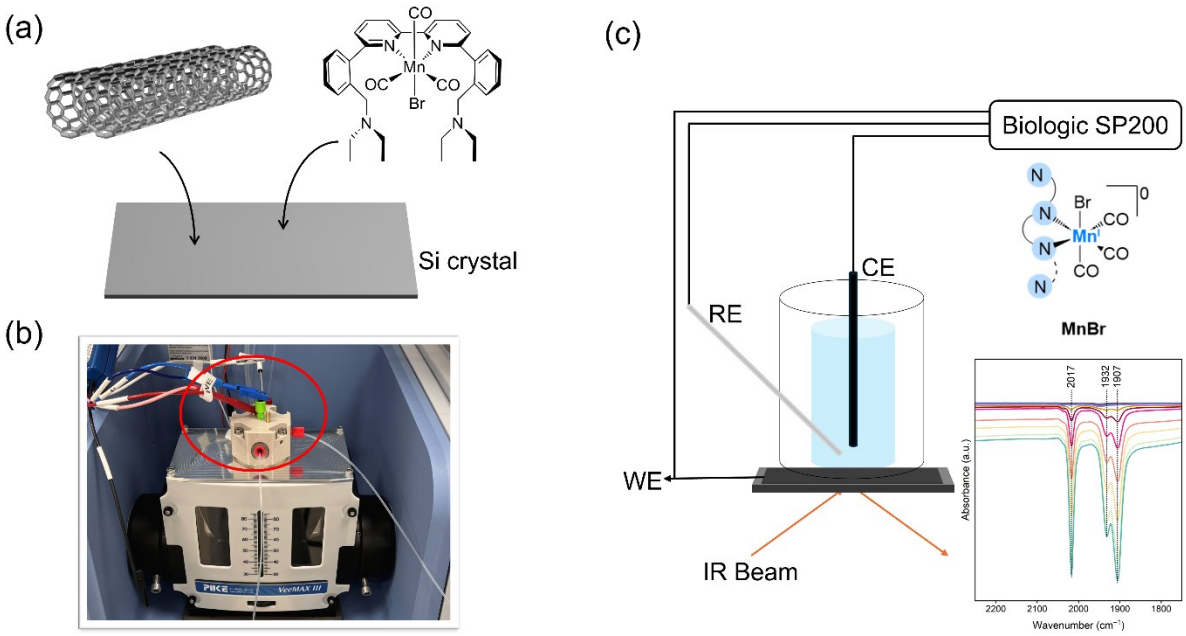

Figure S12. Schematic representation of the ATR-IR SEC experiment. (a) Preparation of the working electrode by coating the Si crystal with an MWCNT film, followed by drop-casting of dissolved complex **I/III** in acetonitrile under dark conditions. (b) Photo of the overall experimental setup: the homemade electrochemical cell was placed on the top of a Pike VeeMAX III specular reflection accessory (angle = 35°) in the sample compartment of a Bruker Invenio R instrument. (c) Schematic diagram of the electrochemical cell internal configuration, highlighted by the circle in (b); the modified prism is mounted into an ATR-IR setup to enable *in situ* recording of IR spectra under potential control.

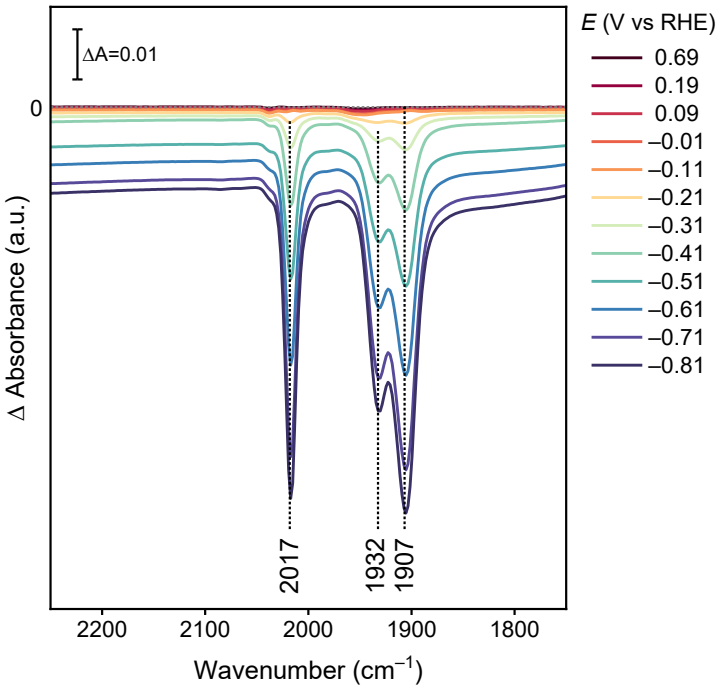

Figure S13. ATR-IR SEC absorbance spectra of **III**/MWCNT recorded at various potentials in Ar-saturated 0.5 M $KHCO_3$ solution. Reference spectrum was collected at 0.69 V vs RHE (0 V vs Ag/AgCl).

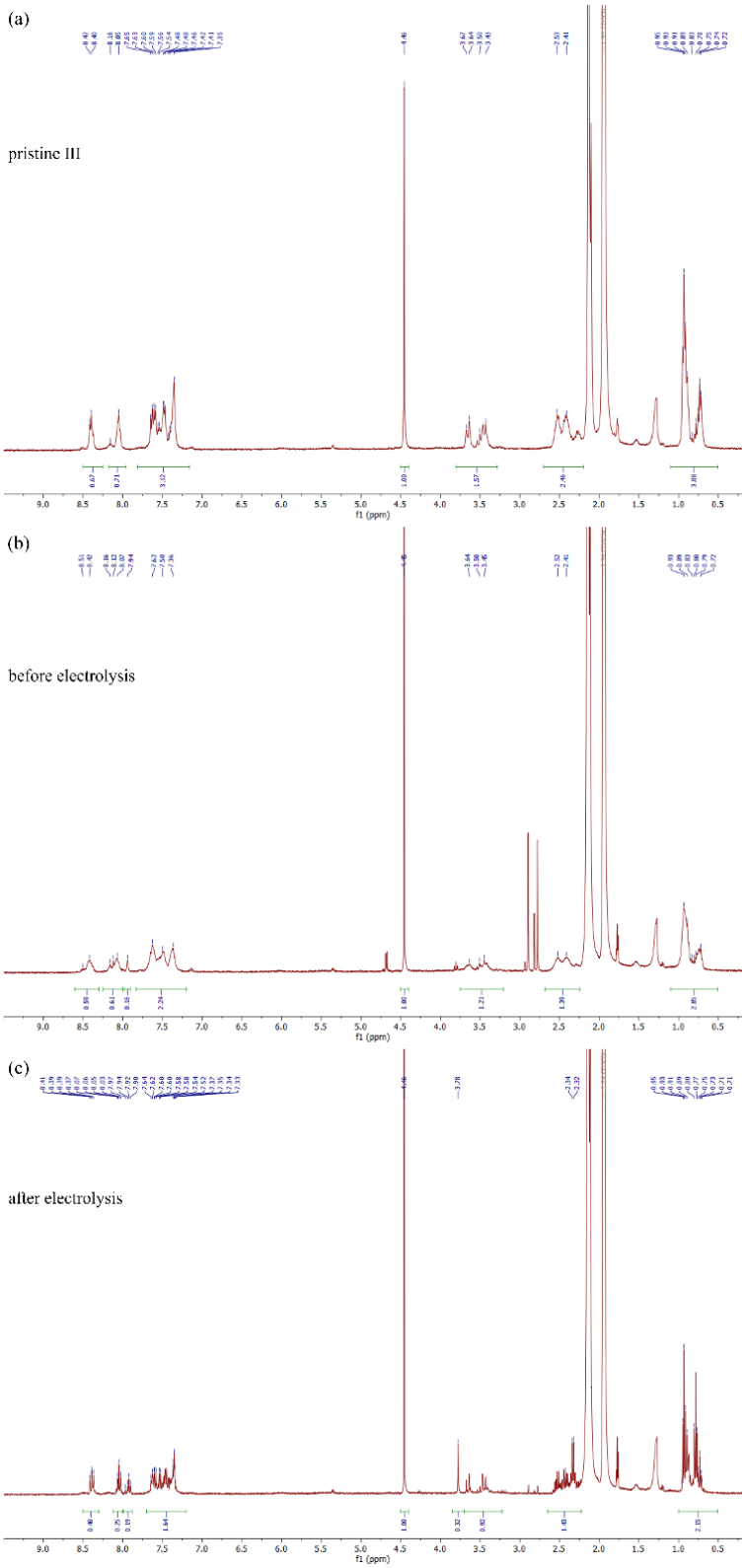

Figure S14. ^{1}H NMR spectra of the complex **III** under different conditions: (a) pristine III in CD_3CN, catalyst rinsed from the **III**/MWCNT-coated carbon paper (b) before and (c) after 8 h of electrolysis at −0.67 V vs RHE.

Post-electrolysis ^{1}H NMR results

To further evaluate the structural integrity of complex **III** after heterogeneous catalysis, we performed additional ^{1}H NMR experiments under three conditions: (i) the pristine complex **III** (1.43mM) dissolved in acetonitrile-d_3 (CD_3CN), (ii) the catalyst recovered from the **III**/MWCNT-coated carbon paper by rinsing with 1 mL CD_3CN before electrolysis, and (iii) the species obtained from the electrode after 8 h of electrolysis at −0.67 V vs RHE using the same rinsing procedure (1 mL CD_3CN). The corresponding spectra are presented in **Figure S14**. Characteristic resonances associated with complex **III** are observed in all three spectra with only minor variations in chemical shift, likely due to solvent exchange, as exemplified by the multiplicity at ~8.4 ppm and ~7.5 ppm. Nevertheless, the singlet at ~3.78 ppm becomes more pronounced in spectrum (c), which is assigned to the benzylic CH_2 protons. This chemical shift of ~3.78 ppm is evidence for the free ligand and is strongly affected by the coordination with the metal center.[S2] The resonance at 3.78 ppm is weak or nearly absent in pristine **III** (**Figure S14a**) and in the sample before electrolysis (**Figure S14b**), consistent with the ligand being coordinated to the Mn center. The enhanced signal after electrolysis, therefore, suggests partial decoordination and decomposition of complex **III** deposited on carbon paper under electrochemical conditions.

Quantitative ^{1}H NMR analysis was performed using ethylene carbonate (10 mM, 50 μL) as an internal standard based on the singlet at ~4.46 ppm (4H). Half of the sample solution (500 μL) was used for analysis. The aromatic multiplet at ~8.4 ppm (2H) was used to quantify intact complex **III** and ligand-containing species, while the resonance at ~3.78 ppm (4H) was used to estimate the amount of ligand uncoordinated with the Mn center. To improve quantification accuracy, larger electrodes (1 × 2 cm) with increased catalyst loading (~0.95 mg per electrode) were used, compared with those used in the electrolysis experiments described in the main text. The concentration of recoverable complex **III** and ligand-containing species decreased from 1.18 mM before electrolysis to 0.80 mM after electrolysis, corresponding to ~32% catalyst leaching from the electrode. In addition, integration of the ~3.78 ppm resonance indicated that ~40% of the recovered species after electrolysis corresponded to free ligand or decomposed ligand-derived species, equivalent to ~27% decomposition relative to the intact complex **III** before electrolysis. The combined catalyst loss from leaching and decomposition (~59%) is in good agreement with the Mn loss determined by ICP analysis of the post-electrolysis electrolyte (**Table S3**), supporting that catalyst deactivation mainly proceeds through dissolution/leaching and partial decomposition of molecular species rather than accumulation of metallic Mn species on the electrode surface.

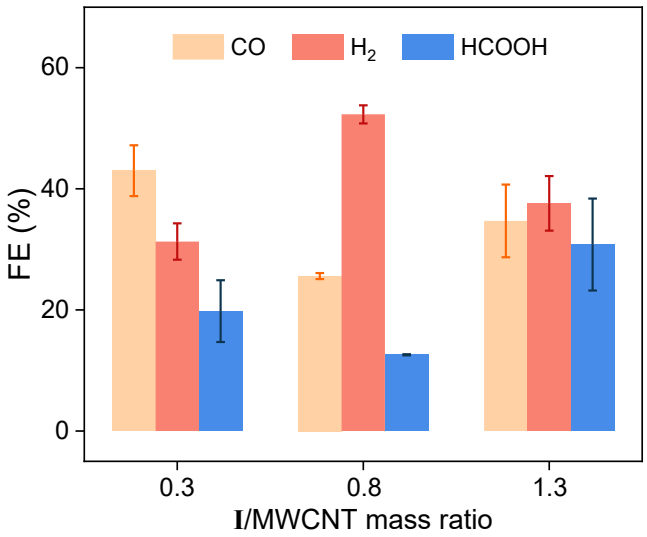

Figure S15. FEs of the CO, H_2, and HCOOH obtained using **I**/MWCNT at various mass ratios at −0.67 V vs RHE after 15 min electrolysis in CO_2-saturated 0.5 M $KHCO_3$. Error bars correspond to the standard deviation of 2–3 independent measurements.

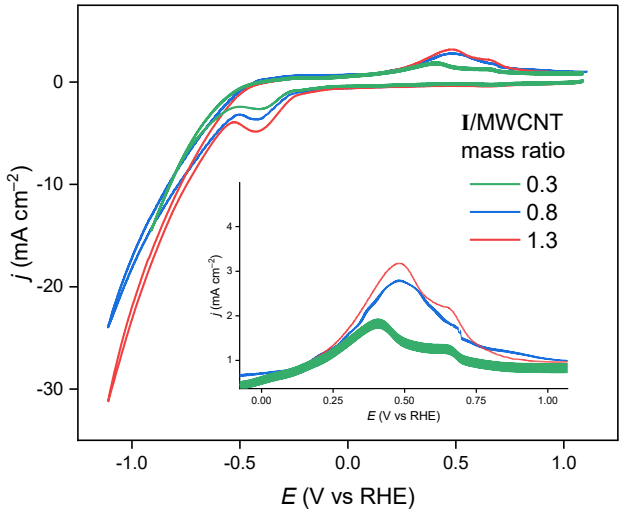

Figure S16. Cyclic voltammograms recorded on **I**/MWCNT at various mass ratios using a sweep rate of 0.1 V s^{-1} in Ar-saturated 0.5 M $KHCO_3$. The inset shows an enlargement of the dimer reoxidation peak.

Quantification of the loading of electrochemically active molecules on the electrode.

Integration of the dimer reoxidation wave in the voltametric sweeps is used to calculate the loading of electroactive molecules using eq S1.

$$\Gamma_{Mn} = \frac{Q}{nFA} = \frac{\sigma}{nF} \qquad \text{(S1)}$$

Here, Γ_{Mn} (mol cm^{-2}) is the loading of electroactive complex **I** per unit electrode area, σ (C cm^{-2}) represents the total charge (Q) transferred per unit electrode area and is obtained from the integration of the oxidation wave (**Figure S16**), n is the number of electrons per Mn center transferred in the redox process (n = 1), F is the Faraday constant (= 96485 C mol^{-1}), and A is the geometric area of the working electrode (= 0.5 cm^2). The results are collected in **Table S4**.

Table S4. Quantification of Loading of Surface-Active Complex **I** on Different Electrodes.

I/MWCNT mass ratio	σ (C cm^{-2})[a]	Γ_{Mn} (mol cm^{-2})[b]	Total loading (mol cm^{-2})[c]	Electroactive fraction (%)[d]
0.3	0.0114	1.18×10^{-7}	5.33×10^{-7}	22.1
0.8	0.015	1.55×10^{-7}	1.33×10^{-6}	11.7
1.3	0.0168	1.74×10^{-7}	2.13×10^{-6}	8.2

[a]σ is the charge transferred per unit electrode area and is obtained by integrating the current density over the potential range of the redox peak. [b]Γ_{Mn} is the surface loading of the electrochemically active complex **I** per unit electrode area. [c]Total loading is calculated based on the amount of complex **I** deposited per unit electrode area. [d]Electroactive fraction is the ratio of Γ_{Mn} to the total loading.

Chart S1. Structures of the Molecules Used in the Heterogenized Catalysts Listed in **Table 1**.

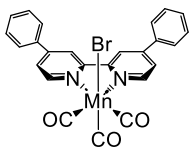

Mn(bpy-ph) MWCNT

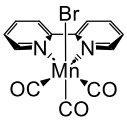

Mn/Nafion/MWCNT

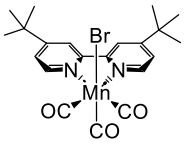

Mn(bpy-tBu)/Nafion/MWCNT

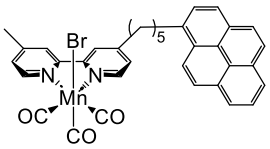

CNT|Mn_{pyr}

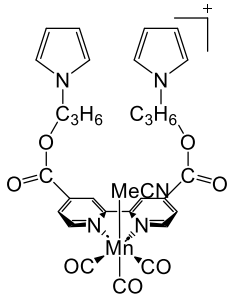

[Mn-MeCN]/MWCNT

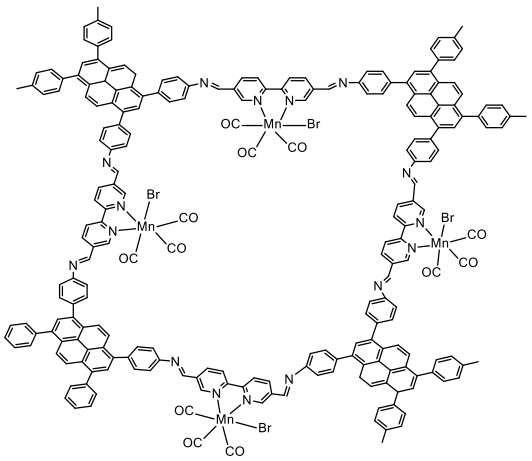

COFbpyMn|CNT

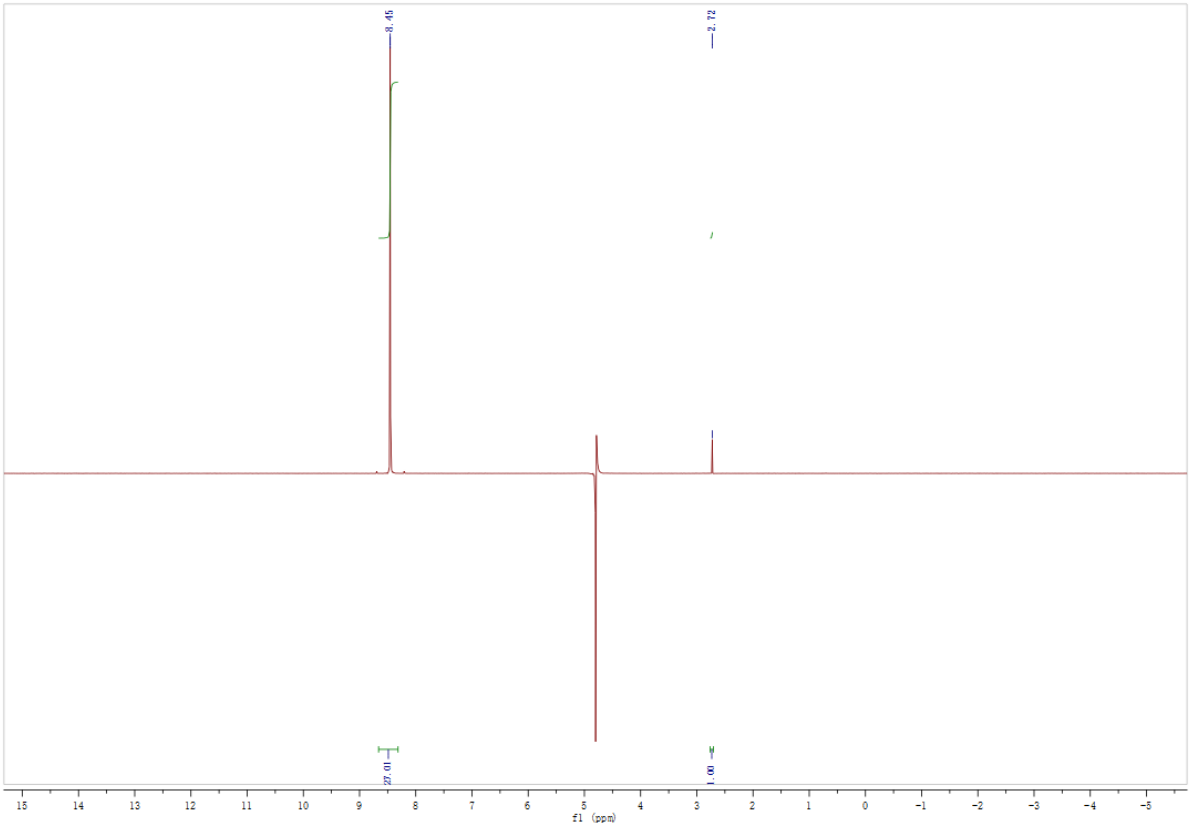

Figure S17. Representative ^{1}H NMR (400 MHz, D_2O) spectrum for the quantification of HCOOH using DMSO as internal standard. The water signal was suppressed using a presaturation sequence.

Figure S17 presents the ^{1}H NMR used to quantify the amount of HCOOH during the 8 h electrolysis present in **Figure 7**. According to the HCOOH quantification procedure, 1 mL of catholyte was mixed with 200 μL of D_2O and 70 μL of 10 mM DMSO/D_2O (internal standard) in a glass sample tube. An aliquot of 635 μL was transferred to an NMR tube, and spectra were acquired with water presaturation. When setting the integral of $(C\underline{\mathbf{H}}_3)_2SO$ to 1, the $\underline{\mathbf{H}}COOH$ integral was observed as 27.01. Following the equation below, the HCOOH concentration in the catholyte was calculated:

$$\frac{A_{DMSO}}{A_{HCOOH}} = \frac{M_{DMSO} \times V_{DMSO} \times 6}{M_{HCOOH} \times V_{HCOOH}} = \frac{10\ mM \times 35\ \mu L \times 6}{M_{HCOOH} \times 500\ \mu L} = \frac{1}{27.01}$$

$$M_{HCOOH} = 113.44\ mM$$

The overall amount of produced HCOOH in the 7.5 mL catholyte was calculated to be:

$$m_{HCOOH} = M_{HCOOH} \times 7.5\ mL = 850.8\ \mu mol$$

Therefore, FE_{HCOOH} (in **Figure 7**) was calculated to be:

$$FE_{HCOOH} = \frac{n \times m_{HCOOH} \times F}{Q} = \frac{2 \times 850.8\ \mu mol \times 96485\ C\ mol^{-1}}{217\ C} = 76\%$$

Here, n (=2) is the number of electrons transferred for CO_2-to-HCOOH conversion, F (= 96485 C mol^{-1}) is the Faraday constant, and Q (= 217 C) is the charge consumed during the 8 h electrolysis.

References

S1. Bourrez, M.; Molton, F.; Chardon-Noblat, S.; Deronzier, A. [Mn(Bipyridyl)$(Co)_3$br]: An Abundant Metal Carbonyl Complex as Efficient Electrocatalyst for Co_2 Reduction. *Angew. Chem. Int. Ed.* **2011**, *50*, 9903–9906.

S2. Rønne, M. H.; Cho, D.; Madsen, M. R.; Jakobsen, J. B.; Eom, S.; Escoudé, É.; Hammershøj, H. C. D.; Nielsen, D. U.; Pedersen, S. U.; Baik, M.-H.; Skrydstrup, T.; Daasbjerg, K. Ligand-Controlled Product Selectivity in Electrochemical Carbon Dioxide Reduction Using Manganese Bipyridine Catalysts. *J. Am. Chem. Soc.* **2020**, *142*, 4265–4275.

S3. Hong, W.; Jakobsen, J. B.; Golo, D.; Madsen, M. R.; Ahlquist, M. S. G.; Skrydstrup, T.; Pedersen, S. U.; Daasbjerg, K. Effect of Variable Amine Pendants in the Secondary Coordination Sphere of Manganese Bipyridine Complexes on the Electrochemical Co_2 Reduction. *ChemElectroChem* **2024**, *11*, e202300553.